Received July 2004
Revised July 2005
Accepted September 2005

# Relationship between thermal convection intensity and aspect ratio of two triangular cavities inscribed in horizontal rectangular cavities

El Hassan Ridouane and Antonio Campo
*Department of Mechanical Engineering, The University of Vermont, Burlington, Vermont, USA*

## Abstract

**Purpose** – Sets out to discuss laminar free convection characteristics of air confined to a square cavity and a horizontal rectangular cavity (aspect ratio $A = 2$) along with the viable isosceles triangular cavities and right-angle triangular cavities that may be inscribed inside the two original cavities.

**Design/methodology/approach** – The three distinct cavities shared the base wall as the heated wall, while the remaining sides and upper walls are cold. The finite volume method is used to perform the numerical computation of the transient conservation equations of mass, momentum and energy. The methodology takes into account the second-order-accurate *quick* scheme for the discretization of the convective term, whereas the pressure-velocity coupling is handled with the *simple* scheme. The working fluid is air, which is not assumed as a Boussinesqian gas, so that all influencing thermophysical properties of air are taken as temperature-dependent. The cavity problem is examined over a variety of height-based Grashof numbers ranging from $10^3$ to $10^6$.

**Findings** – Numerical results are reported for the velocity fields, the temperature field as well as the local and mean wall heat fluxes along the heated base wall. It was found that the airflow remains symmetric for the isosceles triangular cavity with aspect ratio $A = 1$ even at high Grashof numbers. In contrast, for an isosceles triangular cavity with an aspect ratio $A = 2$, a pitchfork bifurcation begins to form at a critical Grashof number of $2 \times 10^5$, breaking the airflow symmetry. The computed local and mean heat fluxes along the hot base wall are compared for the three configurations under study and the corresponding maximum heat transfer levels are clearly identified for the two aspect ratios $A = 1$ and 2.

**Research limitations/implications** – As a continuity of this work, there are two avenues that future research could explore and indeed are presently being explored by the authors within these geometries. The first deals with heat transfer enhancement using mixture of gases. The second is to re-examine the problem under turbulent conditions.

**Originality/value** – The present study seeks to maximize the convection heat transport in cavities and minimize their sizes. The peculiarity of the derived cavities is their cross-section area being half of the cross-section area of the basic cavities.

**Keywords** Cavitation, Numerical analysis, Convection, Heat transfer

**Paper type** Research paper

International Journal of Numerical Methods for Heat & Fluid Flow
Vol. 16 No. 3, 2006
pp. 338-355

0961-5539
DOI 10.1108/09615530610649753

## Nomenclature

| | | | |
|---|---|---|---|
| $A$ | = aspect ratio of cavity ($= L/H$) | $Gr_H$ | = Grashof number ($= g\beta(T_H - T_C)H^3/\nu^2$) |
| $c_p$ | = specific isobaric heat capacity, J/kg K | $h$ | = mean convective coefficient, W/m$^2$K |
| $g$ | = acceleration of gravity, m/s$^2$ | | |

$H$ = height of cavity, m
$L$ = base of the cavity, m
$k$ = thermal conductivity, W/m K
$Nu_H$ = mean Nusselt number ( = $hH/k$)
$p$ = static pressure, Pa
$Pr$ = Prandtl number ( = $\nu/\alpha$)
$q_w$ = local wall heat flux, W/m$^2$
$Q_w$ = mean heat flux, W/m$^2$
$Ra_H$ = Rayleigh number ( = $Gr_H \times Pr$)
$t$ = time, s
$T$ = temperature, K
$T_C$ = cold wall temperature, K
$T_H$ = hot wall temperature, K
$T_r$ = reference temperature ( = $(T_H + T_C)/2$), K
$u, v$ = velocities in the $x$ and $y$ directions, m/s
$x, y$ = horizontal and vertical coordinates, m
$X$ = dimensionless horizontal coordinate ( = $x/L$)
$Y$ = dimensionless vertical coordinate along the mid-plane ( = $y/H$)

*Greek letters*
$\alpha$ = thermal diffusivity ( = $k/\rho c_p$), m$^2$/s
$\beta$ = coefficient of volumetric thermal expansion, 1/K
$\mu$ = viscosity, kg/m s
$\nu$ = kinematic viscosity ( = $\mu/\rho$), m$^2$/s
$\theta$ = dimensionless temperature ( = $(T - T_C)/(T_H - T_C)$)
$\rho$ = density, kg/m$^3$
$\psi$ = stream function ($u = \partial\psi/\partial y, v = -\partial\psi/\partial x$), m$^2$/s

## Introduction

As noted by Gebhart *et al.* (1988), Raithby and Hollands (1998) and Jaluria (2003), the analysis of natural convection of fluids (gases and regular liquids) bounded by square, vertical and horizontal rectangular cavities has been and continues to be an area of considerable interest in engineering, geophysics and environmental sciences. There is a wealth of publications dealing with this kind of two-dimensional cavities thanks to the development of potent grid generation software and efficient computational methods for solving the complete set of Navier-Stokes and energy equations with great precision (Tannehill *et al.*, 1997).

The present paper addresses laminar natural convection of air inside a square cavity (aspect ratio $A = 1$) and a horizontal rectangular cavity (aspect ratio $A = 2$) along with the viable isosceles triangular cavities and right-angle triangular cavities that can be inscribed inside the square and horizontal rectangular cavities. For horizontal rectangular cavities with $A = 2$, Corcione (2003) presented an exhaustive analysis related to heated bottom walls using several cooling combinations in which the other three walls were either insulated or cooled. For the derived isosceles triangular cavities, the two most recent papers that have been reported in the open literature are those of Salmun (1995) and Holtzmann *et al.* (2000) together with the references cited therein. Salmun (1995) examined a two-dimensional right triangular cavity filled with air or water having various aspect ratios and pre-selected Rayleigh numbers. Solutions of the time-dependent conservation equations were obtained using two different numerical techniques which while yielding different numerical values for the velocity and temperature fields, did not altered the flow structure of a single convective cell for low Rayleigh and to multi-cellular regime for high Rayleigh. The finite element method was employed by Holtzmann *et al.* (2000) to model isosceles triangular cavities containing air. These authors used a heated horizontal base and symmetrically cooled upper inclined walls for aspect ratios of 0.2, 0.5 and 1.0 and a variety of Grashof numbers ranging from $10^3$ to $10^5$. In one cavity of fixed aspect ratio, they also conducted a flow visualization study with smoke to validate experimentally the existence of the numerical prediction of the symmetry-breaking pitchfork bifurcations. They also observed that this anomalous phenomenon intensified as

Grashof increased gradually. The major conclusion drawn in this paper was that regardless of the symmetrical and non-symmetrical plumes, the differences in the mean Nusselt number were of the order of 5 percent.

With the dual goal at maximizing the convection heat transport in cavities and minimizing their sizes, the present study seeks to compare the two basic cavities: the square ($A = 1$) and the horizontal rectangle ($A = 2$) against the two derived cavity shapes: the isosceles triangle and the right-angle triangle. The peculiarity of the derived cavities is their cross-section area being half of the cross-section area of the basic cavities.

The body of the present paper is divided into three sections. The three physical systems involving the two basic cavities (square and horizontal rectangular) and the two derived cavities (isosceles and right-angled triangle) and the mathematical formulations are addressed in the first section. The computational procedure and the mandatory validation are explained in the second section. The third section culminates with a discussion of the velocity fields, temperature fields, and total heat transfer rates for the two basic cavities and the two derived cavities.

## Physical systems

The three physical systems under study consist of a horizontal rectangular cavity of variable aspect ratio ($A = 1$ and 2) shown in Figure 1(a), circumscribing an isosceles triangular cavity (Figure 1(b)) and a right-angle triangular cavity (Figure 1(c)). The base, common to the three configurations, is heated with a prescribed high temperature. The remaining walls of each of the three cavities are cooled with a

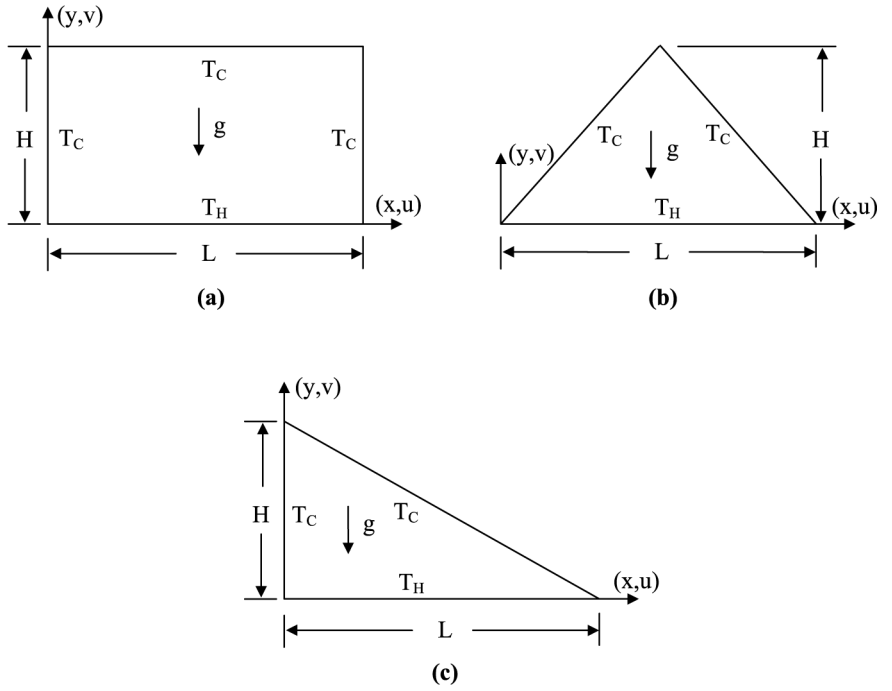


**Figure 1.**
Sketch of a rectangular cavity and the inscribed isosceles and right triangle cavities

prescribed low temperature. The gravitational acceleration acts perpendicular to the base. The dimension normal to the plane of the diagrams is assumed to be long enough, so that the circulatory flows are conceived with two-dimensional motion. The working fluid is air ($Pr = 0.71$). To avoid restrictions imposed by the Boussinesq approximation, the participating thermophysical properties of air such as density, viscosity, specific heat capacity and thermal conductivity are taken as temperature dependent. The set of unsteady conservation equations governing the laminar velocity and temperature fields is:

Mass:

$$\frac{\partial \rho}{\partial t} + \frac{\partial (\rho u)}{\partial x} + \frac{\partial (\rho v)}{\partial y} = 0 \tag{1}$$

Horizontal momentum:

$$\frac{\partial (\rho u)}{\partial t} + \frac{\partial (\rho u u)}{\partial x} + \frac{\partial (\rho u v)}{\partial y} = -\frac{\partial p}{\partial x} + \frac{\partial}{\partial x}\left(\mu \frac{\partial u}{\partial x}\right) + \frac{\partial}{\partial y}\left(\mu \frac{\partial u}{\partial y}\right) \tag{2}$$

Vertical momentum:

$$\frac{\partial (\rho v)}{\partial t} + \frac{\partial (\rho v u)}{\partial x} + \frac{\partial (\rho v v)}{\partial y} = -\frac{\partial p}{\partial y} + \frac{\partial}{\partial x}\left(\mu \frac{\partial v}{\partial x}\right) + \frac{\partial}{\partial y}\left(\mu \frac{\partial v}{\partial y}\right) + (\rho - \rho_r) g \tag{3}$$

Energy:

$$\frac{\partial (\rho T)}{\partial t} + \frac{\partial (\rho c_p u T)}{\partial x} + \frac{\partial (\rho c_p v T)}{\partial y} = \frac{\partial}{\partial x}\left(k \frac{\partial T}{\partial x}\right) + \frac{\partial}{\partial y}\left(k \frac{\partial T}{\partial y}\right) \tag{4}$$

The symbol $\rho_r$ in equation (3) stands for the air density evaluated at a reference temperature $T_r = (T_H + T_C)/2$.

The velocity boundary conditions are based on the assumptions that all cavity walls are rigid and impermeable and also that the moving fluid does not slip at the walls. Prescribed temperature boundary conditions are imposed at the heated and cooled walls.

## Numerical computations

To preserve uniformity, the computational domains are coincident with the physical domains in the three different cavities. Finite-volume solutions of equations (1)-(4), subject to the imposed boundary conditions determine the laminar velocity and temperature fields in the air-filled cavities under the influence of appropriate height-based Grashof numbers. The finite volume method is used to perform the numerical calculations within the FLUENT code platform (*FLUENT Reference Manual*, 2002). In this framework, the second-order-accurate *quick* and *simple* schemes facilitate the discretization of the convective term and the pressure-velocity coupling in the conservation equations (1)-(4).

Based on a sequence of numerical experiments, it was found that the optimal computational mesh that renders grid independent solutions consists of 20,000 quadrilateral elements for the square and the rectangular cavities and 62,000 triangular elements for the isosceles and the right triangular cavities. Care was taken to increase the element density in sensitive areas where pronounced velocity and temperature

gradients would occur, such as near the walls with special emphasis in the wall intersections. The grid layouts chosen rendered reliable air velocity and temperature fields for the selected Grashof numbers in the interval $10^3 \leq Gr_H \leq 10^6$. Grid independence was achieved within one percent for the six cavities at the highest Grashof number, i.e. $Gr_H = 10^6$.

Local convergence was assessed by monitoring the magnitude of mean convective coefficient $h$ along the heated base wall, whereas global convergence was guaranteed by controlling the residuals of the conservation equations (1)-(4). The criteria adopted for the convergence of the laminar velocities and temperature fields is the norm:

$$\frac{1}{\phi_{\max}} \sqrt{\sum_{i=1}^{N} \left(\phi_i^{n+1} - \phi_i^n\right)^2} \leq \varepsilon \tag{5}$$

where typically $\varepsilon = 10^{-4}$. It was noticed that further decreases in $\varepsilon$ do not cause any significant changes in the numerical results. Additionally, the overall energy balance, written in terms of the integrated heat transfer rate through the thermally active walls is equal. After the convergence of the velocity and temperature fields was attained, the streamlines and isotherms were calculated.

The local wall heat flux along the hot base wall $q_w(x)$ was found by applying Fourier's law at this wall which is common to the basic and derived cavities. This step leads to the computation of the mean wall heat flux $Q_w$ along the hot base wall:

$$Q_w = \frac{1}{L} \int_0^L q_w(x) \mathrm{d}x \tag{6}$$

Subsequently, the mean Nusselt number $Nu_H$ is obtained from the relation:

$$Nu_H = \frac{Q_w H}{k(T_H - T_C)} \tag{7}$$

where the air thermal conductivity $k$ is evaluated at the reference temperature $T_r = (T_H + T_C)/2$.

Two validations of the numerical code have been done. First, using a reference square cavity with hot and cold vertical sidewalls and two insulated horizontal walls. At the local level, the magnitude of the dimensionless vertical velocity $V_{\max} = 221.80$ at a relatively high value $Ra_H = 10^6$ is within 5 percent of the benchmark results of 217.36 by De Vahl Davis (1983). Also at the global level for $Ra_H = 10^6$, agreements to less than 1 percent of the mean Nusselt number $Nu_H = 8.75$ in this work vs 8.799 by De Vahl Davis (1983) are obtained. Second, employing the experimental measurements in an isosceles triangle conducted by Flack (1980). We chose an isosceles triangle holding an intermediate apex angle of 45° between the bottom wall and the inclined walls as representative. Figure 2 shows the excellent parity between the experimental and the numerical Nusselt numbers $Nu_H$ for both heating/cooling scenarios. For case 1 (hot upper walls and cold bottom wall), the invariance of $Nu_H$ with the Grashof number $Gr_H$, staying around 4.63, indicates that the heat is transported by conduction. For case 2 (cold upper walls and hot bottom wall), $Nu_H$ exhibited a power law dependence with $Gr_H$. The maximum deviation between the numerical and experimental Nusselt number is within 3.5 percent for both cases.

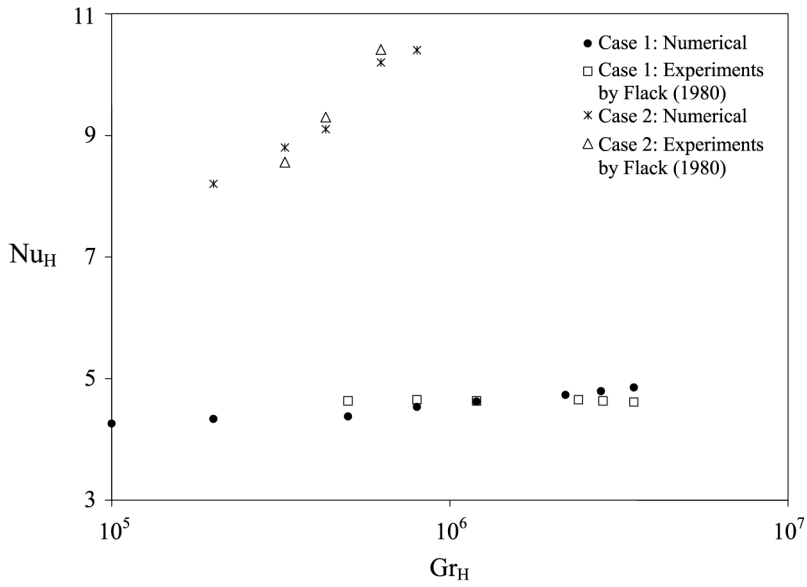


**Figure 2.**
Comparison between the numerical and experimental mean Nusselt numbers within an isosceles triangular cavity for case 1 (hot upper walls and cold base) and case 2 (cold upper walls and hot base)

## Discussion of numerical results

The six closed spaces filled with air, the square and the rectangle (RE), the two isosceles triangle cavities (IT) and the two right-angle triangle (RT) cavities sharing the same hot base are shown in Figure 1. It is worth recognizing that the size of the IT and RT cavities are equivalent to half of the square and rectangular cavities with different shapes. The base wall is held at $T_H$ and the remaining walls are held at $T_C$ with $T_H > T_C$. The Prandtl number has been fixed to 0.71, and the Grashof number ranged from $10^3$ to $10^6$. First, the flow and temperature fields, as well as the heat transfer rates are examined for the square cavity owing an aspect ratio $A = 1$. This format is repeated for the rectangular cavity having an aspect ratio $A = 2$. Later, the effect of the aspect ratio on the thermo-fluid performance of the group of cavities are presented and discussed. Also, the main objective in every case ($A = 1$ and 2) is to search for the original or derived geometries that are capable of maximizing the global heat transfer across the cavity when dividing the square and rectangular cavities in half.

*Case 1: cavities with $A = 1$*

The streamlines and isotherms for $Gr_H = 10^3$ and $10^6$ are shown in Figures 3 and 4. In all the streamline plots, the contour lines correspond to equispaced absolute values of the stream function $\psi$. Likewise, in all the isotherm plots, the contour lines correspond to equispaced values of the temperature $T(x, y)$ in the range between 287 and 313 K.

At $Gr_H = 10^3$, the fluid systems are placed slightly above the critical state, which corresponds to the onset of thermal convection. The critical Grashof number for the three geometries lies approximately between $10^2$ and $10^3$. The steady-state patterns are characterized by two counter rotating vortices. It is observable that this solution is symmetric for the square and the IT cavities. The convective motion is oriented upward in the central region (hot stream) and downward near the sidewalls (cold stream). The strength of the vortices rotation can be determined by calculating

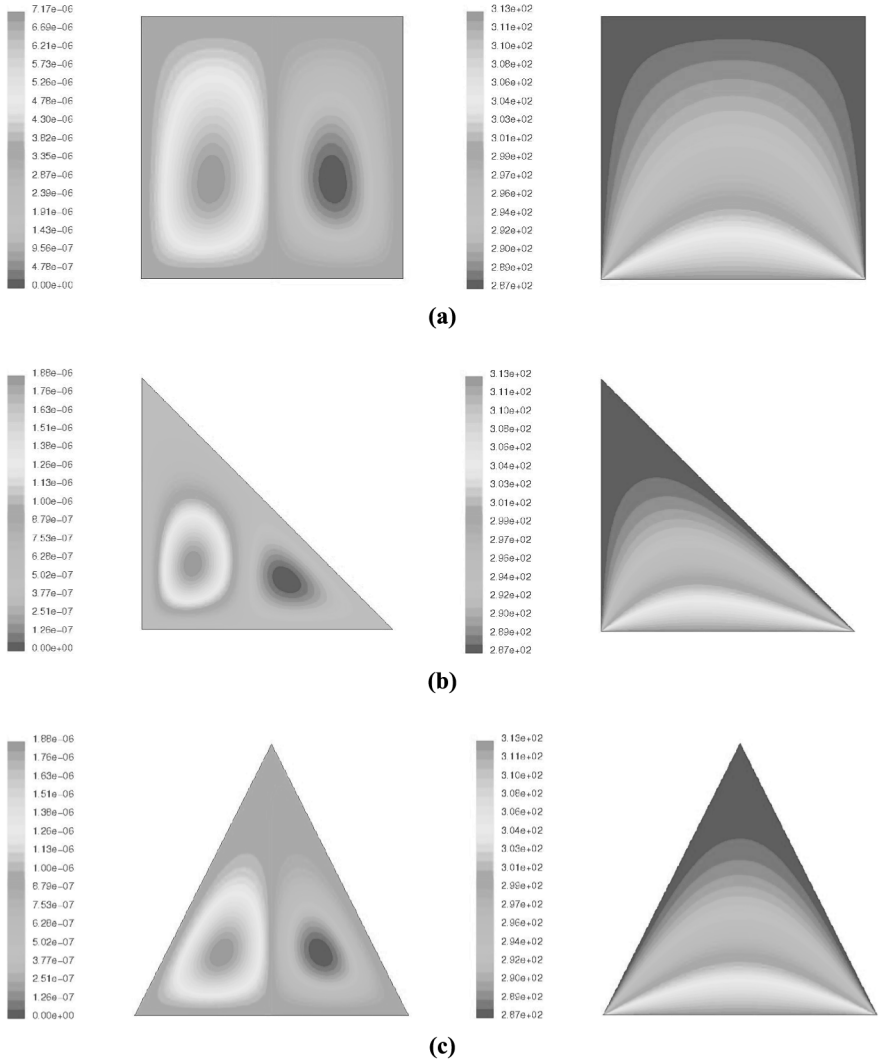


**Figure 3.**
Plots of stream functions and isotherms for $A = 1$ and $Gr_H = 10^3$

the magnitude of the stream function gradient. The RE cavity displays the largest magnitude for the stream function gradient, while the IT and RT cavities display the smallest. Therefore, as expected the vortices strength and velocities reach highest values for the square and lowest for the IT and RT cavities. The isotherms are almost straight over the whole length of the cavities indicating that the process of heat transfer across the cavities is basically dominated by conduction. When $Gr_H$ is increased to $10^6$, the qualitative shape of the counter rotating cells remains the same as shown in Figure 4. However, the magnitude of the velocity gradients increases by three orders of magnitude creating as a result higher fluid velocities. Consequently, this trend indicates that convection is progressively dominating the process of heat

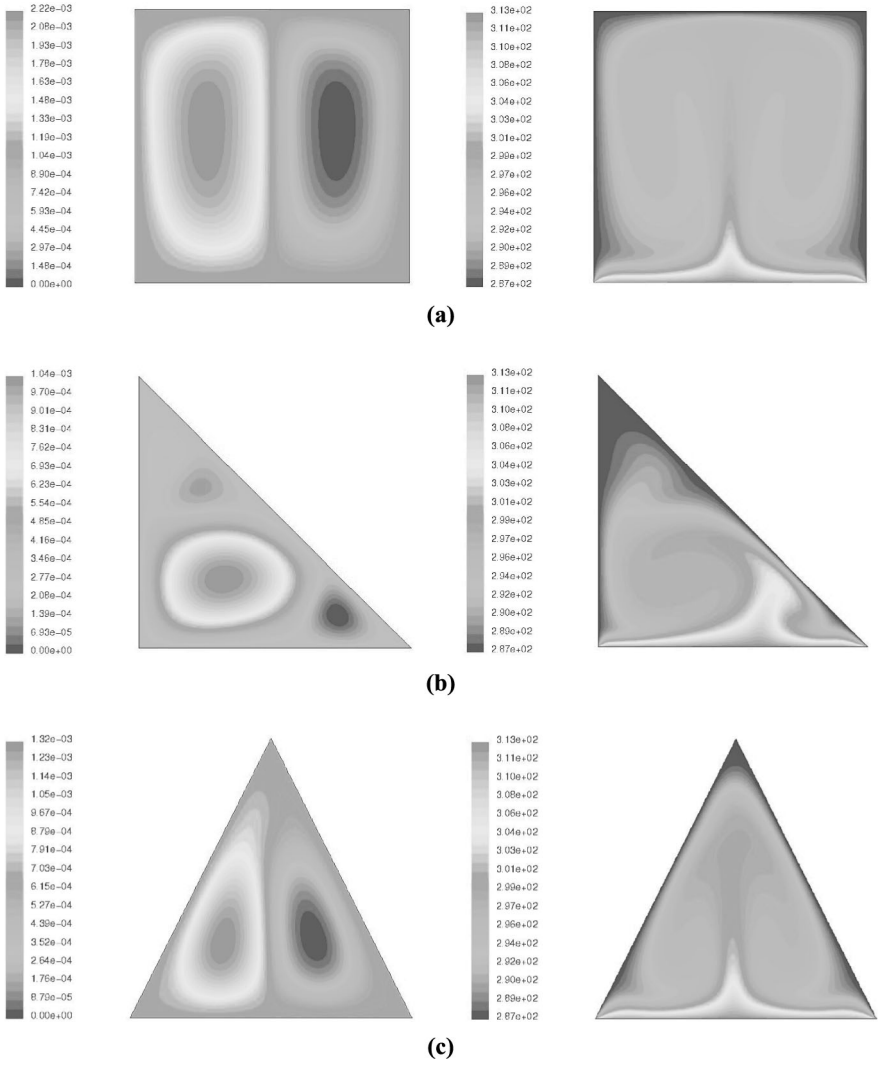


**Figure 4.**
Plots of stream functions and isotherms for $A = 1$ and $Gr_H = 10^6$

transfer. The strength of the vortices is also increased as seen by the magnitude of the stream function gradient. Regarding the results divulged by Holtzmann *et al.* (2000), these authors discovered the formation of a symmetry-breaking pitchfork bifurcation, which occurs at a certain critical Grashof for each aspect ratio considered. The flow symmetry in the IT is not affected by increments in the $Gr_H$ for $A = 1$ and the flow structure remains symmetric even at high $Gr_H = 10^6$. The isotherms become more complex, since the natural convection term dominates the conduction term, and tends to transport the hottest fluid above the coldest fluid.

Figure 5 shows the variation of the dimensionless temperature along the mid-plane of the three cavities for an intermediate Grashof number of $Gr_H = 10^5$. The thermal

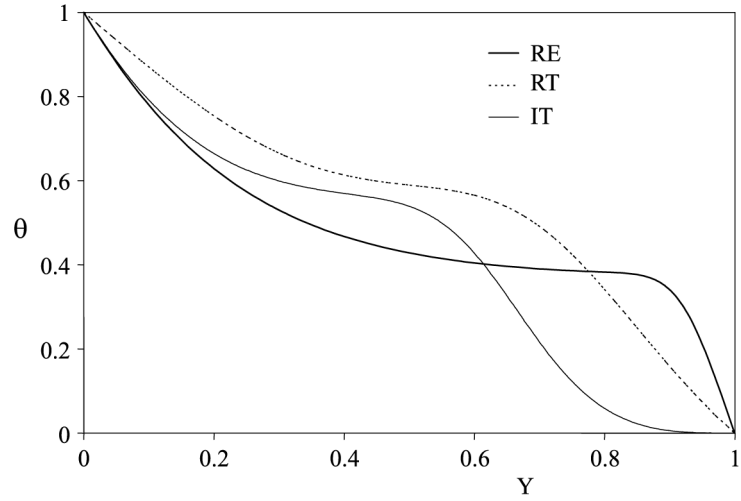


**Figure 5.**
Dimensionless temperature profiles along the mid-plane for $A = 1$ and $Gr_H = 10^5$

boundary layer grows close to the hot wall when moving from the square to the IT cavities and the horizontal temperature at the center of the cavity is reduced from $\theta = 0.62$ for the RT to $\theta = 0.59$ for the IT to $\theta = 0.42$ for the square. In this case, the pure convection solution is greatly affected by the shape of the cavity in the central part since the temperature distribution is not only flattened but also shifted downward.

In Figure 6, typical local heat fluxes are presented ($Gr_H = 10^5$) for the heated bottom wall. The results are illustrated for the three configurations considered. For small values of $X$, $q_w$ begins with a relatively large value at the point where the temperature discontinuity $X = 0$ occurs. The magnitude of $q_w$ is typically 300 and 200 percent higher than for the simple square geometry in the cases of RT and IT, respectively.

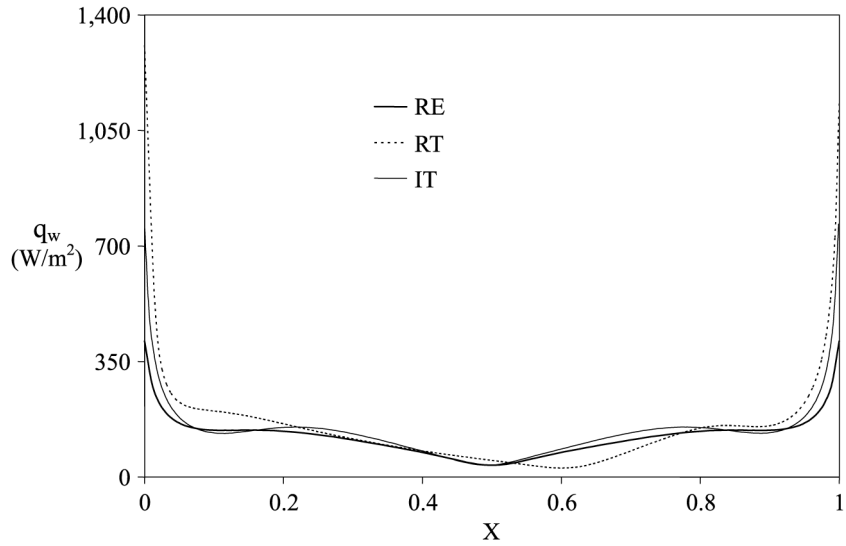


**Figure 6.**
Surface heat flux $q_w$ along the hot base wall for $A = 1$ and $Gr_H = 10^5$

As $X$ grows, $q_w$ exhibits a positive skewed concave U-shape with respect to the abscissa $X$. In the sub-interval $0.05 \leq X \leq 0.95$, $q_w$ stays almost constant showing subtle variations. This comportment is indicative that considerable thermal convection has occurred. Further, it is notorious that the $q_w$ curve for the RT is the highest as opposed to the lowest for the RE cavity. This behavior translates into a large heat transfer rate across the RT cavity when compared against the heat transfer rate across either the basic square or derived IT cavity.

In Figure 7, the height-based mean Nusselt number $Nu_H$ is plotted versus the logarithm of the $Gr_H$ number for the three interrelated cavities that originate in the square cavity. Conceivably, the lowermost $Nu_H$ curve representative of the square cavity demonstrates the monotonic increase of $Nu_H$ with increments in $Gr_H$ number. This cavity constitutes the natural baseline case for comparison purposes. When the square cavity is split in half as shown in Figure 1, we obtain the RT and the IT cavities. The cross-section areas of both are half of the cross-section area of the square. The overall response of $Nu_H$ to changes in $Gr_H$ for the joined RT and IT cavities may be viewed as the intersection of a horizontal straight line for $Gr_H \rightarrow 0$ and a positive sloped straight line for $Gr_H \rightarrow \infty$. The point of intersection of these two lines lies around a critical $Gr_H \approx 7 \times 10^3$, which clearly identifies the onset of natural convection. By visual inspection of the curves in Figure 7, it is revealed that the RT cavity is better than the IT cavity, and that the IT cavity outperforms the square cavity. Qualitatively speaking, the items in Table I confirm the superiority of the RT cavity with respect to the IT cavity. Although the heat transfer enhancement of the RT cavity relative to the square cavity is of the order of 64 percent at $Gr_H = 10^3$, it is diminishing in approximately half to 29 percent at $Gr_H = 10^6$. Since the cold perimeter of a square cavity is 3 units, the companion Table II elucidates a saving in cold perimeter of 20 percent brought forward the RT cavity. Presumably, this incremental heat transfer may be attributed to the large cold perimeter of 2.41 units in the RT cavity as compared to a small cold perimeter of 2.24 units for the IT cavity.

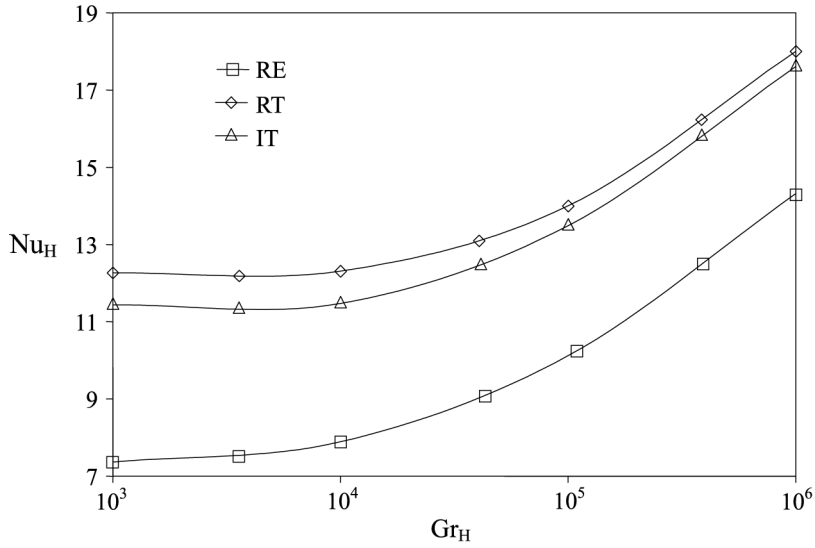


**Figure 7.**
Variation of the mean Nusselt number $Nu_H$ with Grashof number $Gr_H$ for $A = 1$

*Case 2: cavities with $A = 2$*

Isotherm and streamline contour plots relevant to the trio of RE, RT and IT cavities are shown in Figure 8 for $Gr_H = 10^3$ and the aspect ratio $A = 2$. It may be noticed that the flow structure remains the same as shown in Figure 3. However, the strength of the rotating vortices was found to be higher for $A = 2$ when compared against the base case with $A = 1$. This pattern suggests that natural convection starts at very early Grashof numbers for $A = 2$. As Grashof number increased to $8 \times 10^5$, the circulation patterns for the RT and IT cavities are radically changed and stayed symmetric for RE cavity. For the RT cavity, secondary vortices appear in the right corner of the cavity as shown in Figure 9(b). These new vortices push the main vortex towards the center and contribute to increase the heat transfer across the cavity. As the Grashof number is invigorated to $8 \times 10^5$, four rotating cells showed up in the IT cavity; this can be seen in Figure 9(c). These new cells again move warm fluid from the hot wall and help to enlarge the overall heat transfer. In addition to the new vortices formation, the strength of the original vortices is higher compared to the base case shown in Figure 4. The direct effect of these new vortices on the temperature field can be seen on the isotherm plots, where two streams of warm fluid are directed upward from the hot wall.

The centerline temperature profiles are shown in Figure 10 for an intermediate Grashof number $Gr_H = 10^5$. In this figure, large temperature drops are manifested near the top and bottom of the cavity, i.e. in the thermal boundary layer. The remaining central portion of the cavities remains almost isothermal and the temperature at the center of the cavity is reduced from $\theta = 0.69$ for the RT to $\theta = 0.56$ for the IT to $\theta = 0.47$ for the RE cavity. When compared to the base case, we should expect subtle temperature changes in the central region of the cavities, and as a consequence, the shape of the temperature profiles persists.

The effect of the aspect ratio upon the local heat flux along the hot base is shown in Figure 11, where $q_w$ is plotted vs the coordinate along the base for each geometry sharing $A = 2$. Again $q_w$ begins with large value at the point where the discontinuity $X = 0$ occurs. This value is highly affected by the increase of the aspect ratio.

**Table I.**
Heat transfer enhancement of the inscribed triangular cavities with respect to the square cavity

| | $Gr_H = 10^3$ | Heat transfer enhancement (percent) | $Gr_H = 10^6$ | Heat transfer enhancement (percent) |
|---|---|---|---|---|
| Square (RE) | $Nu_H = 7.3$ | – | $Nu_H = 14$ | – |
| Isosceles triangle (IT) | $Nu_H = 11.5$ | 58 | $Nu_H = 17.5$ | 25 |
| Right-angle triangle (RT) | $Nu_H = 12$ | 64 | $Nu_H = 18$ | 29 |

**Table II.**
Relationship between the cold perimeters of the square cavity and the two inscribed triangular cavities

| | Cold perimeter (units) | Cold perimeter saving (percent) |
|---|---|---|
| Square (RE) | 3 | – |
| Isosceles triangle (IT) | 2.24 | 25 |
| Right-angle triangle (RT) | 2.41 | 20 |

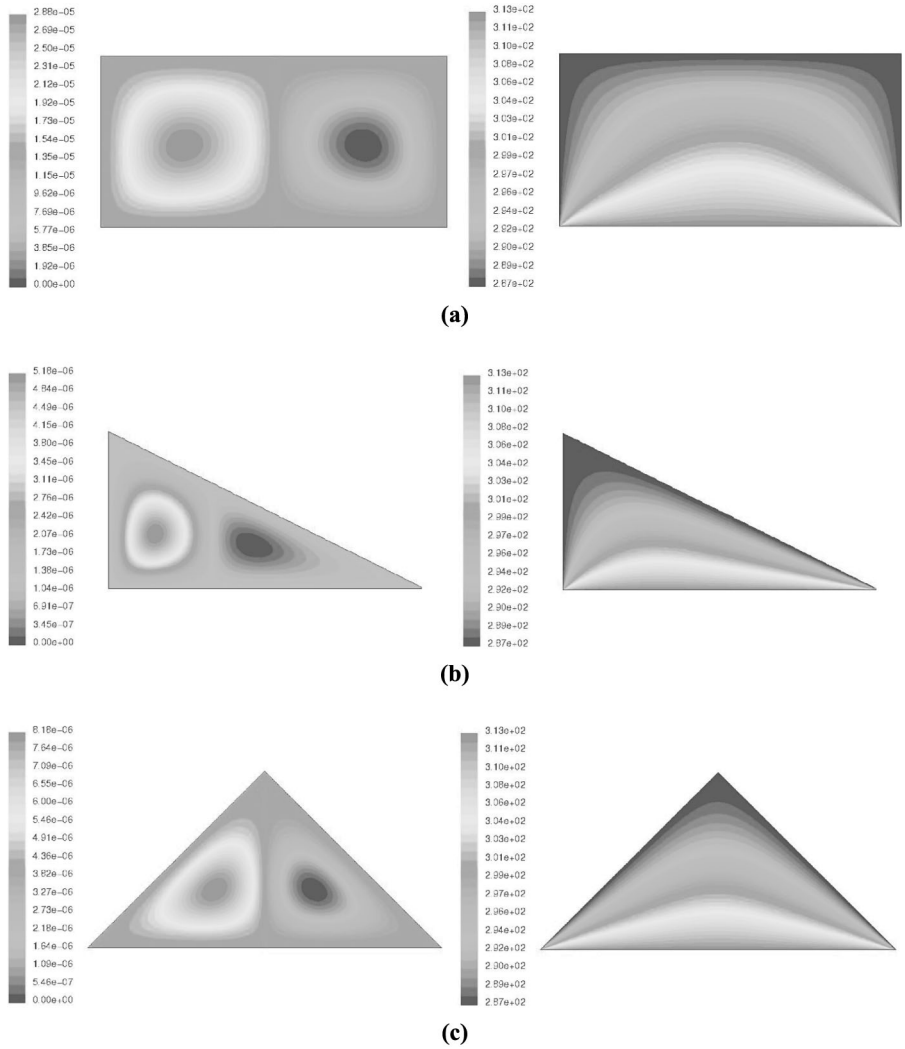


**Figure 8.**
Plots of stream functions and isotherms for $A = 2$ and $Gr_H = 10^3$

Compared to the base case, $q_w$ decreases from 1,300 to 700 W/m$^2$ for the RT, from 800 to 750 W/m$^2$ for the IT and from 420 to 250 W/m$^2$ for the RE cavity. As $X$ increases $q_w$ decreases quickly in the sub-interval $0 \leq X \leq 0.05$. After that, the $q_w$ curve is almost constant in the sub-interval $0.05 \leq X \leq 0.95$ but is characterized by the presence of peaks. Each peak is the result of an upward stream between two rotating vortices, which remove heat from the hot wall and contribute to the overall heat transfer across the cavity. Clearly, the magnitude of each peak is proportional to the strength of the corresponding vortex. Approaching to the $X = 1$ discontinuity, $q_w$ increases quickly to reach high values indicating that a sizable heat transfer has occurred by conduction in this region. It is worth mentioning here that when $A$ climbs to 2, $q_w$ turns out to be the

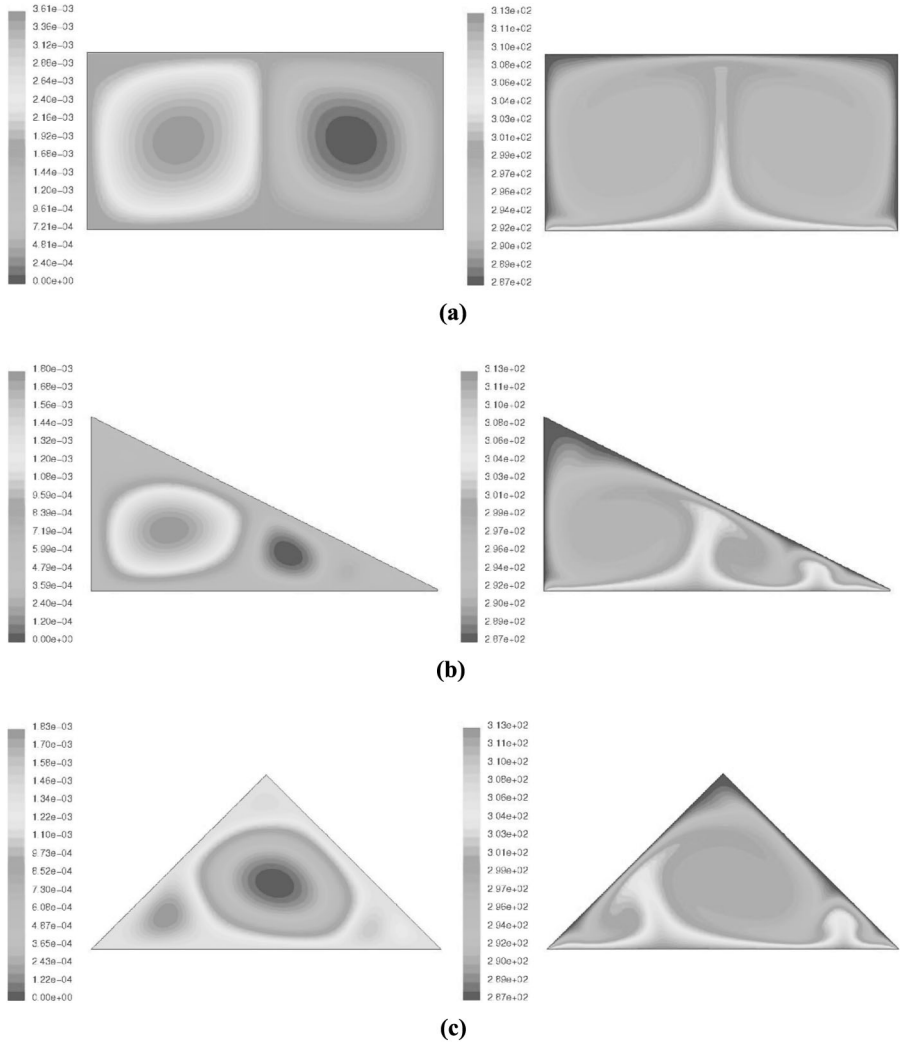


**Figure 9.**
Plots of stream functions and isotherms for $A = 2$ and $Gr_H = 8 \times 10^5$

highest for the IT case, intermediate for the RT case and the lowest for the RE case. This sequential pattern opposes the one for the base case where the RT exhibits the largest local heat flux along the hot wall.

The wall heat flux predictions $q_w$ vs $X$ associated with various $Gr_H$ were transformed into mean Nusselt number $Nu_H$ and the outcome is plotted later in Figure 12. It can be seen in this figure that the shape of the $Nu_H$ family of curves for $A = 2$ follows the footsteps of its counterpart for $A = 1$ in Figure 7. However, as $A$ doubled from 1 to 2, $Nu_H$ gets reduced.

Shown in Figure 12 is the height-based mean Nusselt number $Nu_H$ varying with the logarithm of the $Gr_H$ number for the three interrelated cavities that originate in the

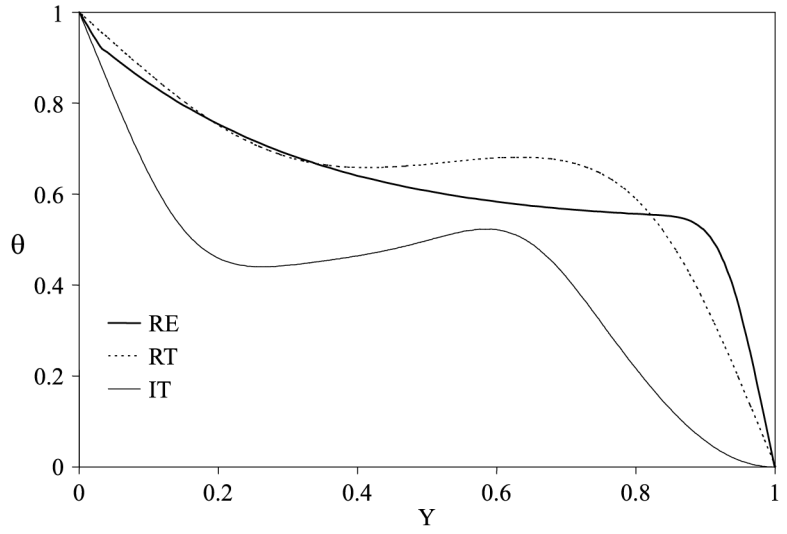


**Figure 10.**
Dimensionless temperature profiles along the mid-plane for $A = 2$ and $Gr_H = 10^5$

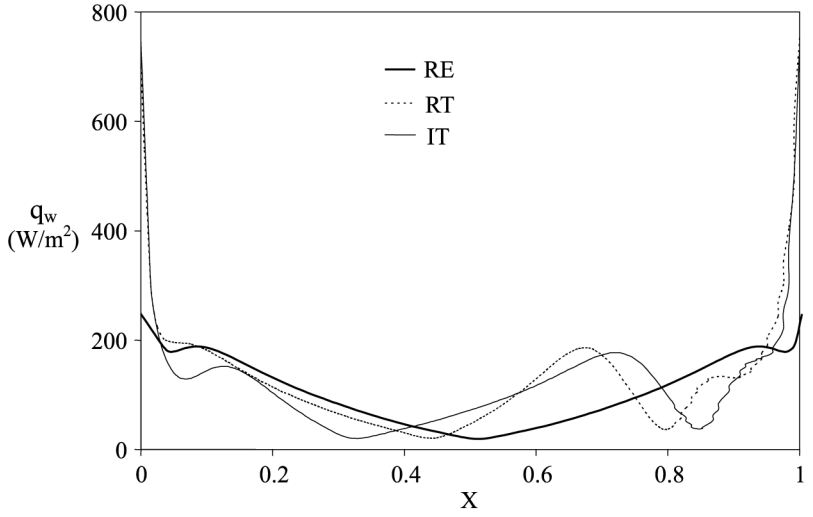


**Figure 11.**
Surface heat flux $q_w$ along the hot base wall for $A = 2$ and $Gr_H = 10^5$

horizontal rectangular cavity. Again, the lowermost $Nu_H$ curve representative of the rectangular cavity ascends monotonically with increments in $Gr_H$ number. This cavity constitutes the natural baseline case for comparison purposes. When the rectangular cavity is split in half as shown in Figure 1, we obtain the inscribed RT and IT cavities. As before, the cross-section areas of both are half of the cross-section area of the rectangular cavity. The overall response of $Nu_H$ to changes in $Gr_H$ for the joined RT and IT cavities may be viewed as the intersection of a horizontal straight line for $Gr_H \rightarrow 0$ and a positive sloped straight line for $Gr_H \rightarrow \infty$. The point of intersection of these two lines lies around a critical $Gr_H \approx 10^4$, which clearly identifies the onset of

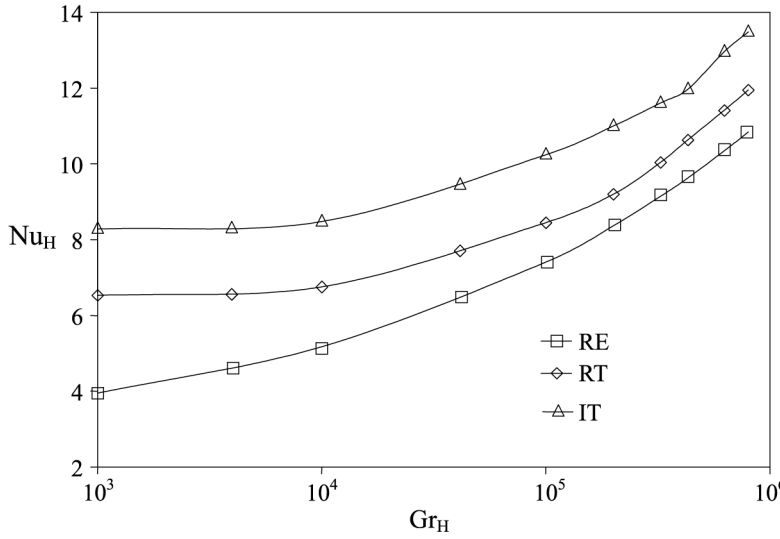


**Figure 12.**
Variation of the mean Nusselt number $Nu_H$ with Grashof number $Gr_H$ for $A = 2$

natural convection. By visual inspection of the curves in Figure 12, it is revealed that in this case the IT cavity is better than the RT cavity, and that the RT cavity outperforms the rectangular cavity. From a qualitative perspective, an inspection of the items in Table III reveals the superiority of the IT cavity with respect to the RT cavity. Although the heat transfer enhancement of the IT cavity relative to the rectangular cavity yields a remarkable 108 percent at $Gr_H = 10^3$, it diminishing in approximately a quarter to 27 percent at $Gr_H = 10^6$. Since the cold perimeter of a rectangular cavity is 4 units, it can be seen in the companion Table IV that the IT cavity brought forward a saving in cold perimeter of 29 percent. Supposedly, a larger cold perimeter of 2.83 units

**Table III.**
Heat transfer enhancement of the inscribed triangular cavities with respect to the horizontal rectangular cavity ($A = 2$)

| | $Gr_H = 10^3$ | Heat transfer enhancement (percent) | $Gr_H = 10^6$ | Heat transfer enhancement (percent) |
|---|---|---|---|---|
| Rectangle (RE) | $Nu_H = 4$ | – | $Nu_H = 11$ | – |
| Right-angle triangle (RT) | $Nu_H = 6.5$ | 63 | $Nu_H = 12.5$ | 14 |
| Isosceles triangle (IT) | $Nu_H = 8.3$ | 108 | $Nu_H = 14$ | 27 |

**Table IV.**

| | Cold perimeter (units) | Cold perimeter saving (percent) |
|---|---|---|
| Rectangle (RE) | 4 | – |
| Right-angle triangle (RT) | 2.24 | 44 |
| Isosceles triangle (IT) | 2.83 | 29 |

**Note:** Relationship between the cold perimeters of the horizontal rectangular cavity ($A = 2$) and the two inscribed triangular cavities

in the IT cavity as compared to a small cold perimeter of 2.24 units for the RT cavity may be the cause for the incremental heat transfer.

A side comment could be added. In the event that extra heat needs to be transferred in the derived cavities, regardless of the aspect ratio the sharp wall intersections can be curved as suggested by Campo and Ridouane (2005).

*Unsteady analysis*

Responding to a question raised by the referee, the temporal distortion of the plume is explained now. For the IT cavity, beginning with $Gr_H = 10^3$, as the Grashof number is increased, the symmetric plume disappears and a pitchfork bifurcation is created at a critical value of Grashof number, say $Gr_{H,C}$. Above this critical value, two steady-state solutions are possible; the first is plotted in Figure 9(c) and the second is the image of the first through a vertical mirror which is characterized by cells rotating in opposite directions when compared to the first solution. The critical value $Gr_{H,C} = 2 \times 10^5$ is obtained for the IT cavity with $A = 2$. Particular care was taken in order to show how the temporal changes triggered by the flow structure, underwent. Unsteady calculations were performed to illustrate the flow structure evolution with time at $Gr_H = Gr_{H,C}$. The initial perturbations at $t = 0$ come from the symmetrical steady-state solution at $Gr_H = 10^5$. The flow visualization in terms of isotherms is plotted at selected times during the transition and the outcome is shown in Figure 13. At $t = 76.6$ min, Figure 13(a) shows that the flow is still symmetrical with respect to the mid-plane. Slight deformations are observed when $t$ reaches the value of 146.7 min. At this instant, the right cell increased and passed the mid-plane while the left cell remains in the corner but diminishes in size (Figure 13(b)). This behavior intensifies with time; the right clockwise cell dominates over the left cell when time increases. Figure 13(c) and (d) shows the evolution of the isotherms at $t = 183.5$ and 228.3 min, respectively. This behavior continues until the flow patterns reach the new steady-state at $t = 293.1$ min. Further increments in time do not affect the flow and temperature distribution. The final steady-state condition at $Gr_H = 2 \times 10^5$ is shown in Figure 13(e) at $t = 395.8$ min.

## Concluding remarks

The study of natural convection heat transfer in air-filled square and horizontal rectangular cavities with aspect ratio $A = 2$ in conjunction with two viable isosceles triangular cavities and right-angle triangular cavities inscribed inside the square and horizontal rectangular cavities has been studied numerically. Limited experimental validation has been provided. The compounded effects of the aspect ratio and the Grashof number on the steady-state solutions for each geometry are investigated in detail. Whenever $A = 1$, symmetric velocity and temperature fields are obtained for the square and IT cavities covering the entire range of $Gr_H$ explored, namely ($10^3$-$10^6$). However, as $A$ is enlarged to 2, the plume symmetry breaks down and disappears in the case of the IT cavity. Thereafter, a pitchfork bifurcation creates an anti-symmetric plume at a critical Grashof number, $Gr_{H,C} = 2 \times 10^5$. The evolution of the flow structure with time is reported in detailed form to illustrate how this physical transition manifests. At high Grashof numbers, secondary vortices appear for the RT and the IT cavities being instrumental in the intensification of the overall heat transfer across the cavity.

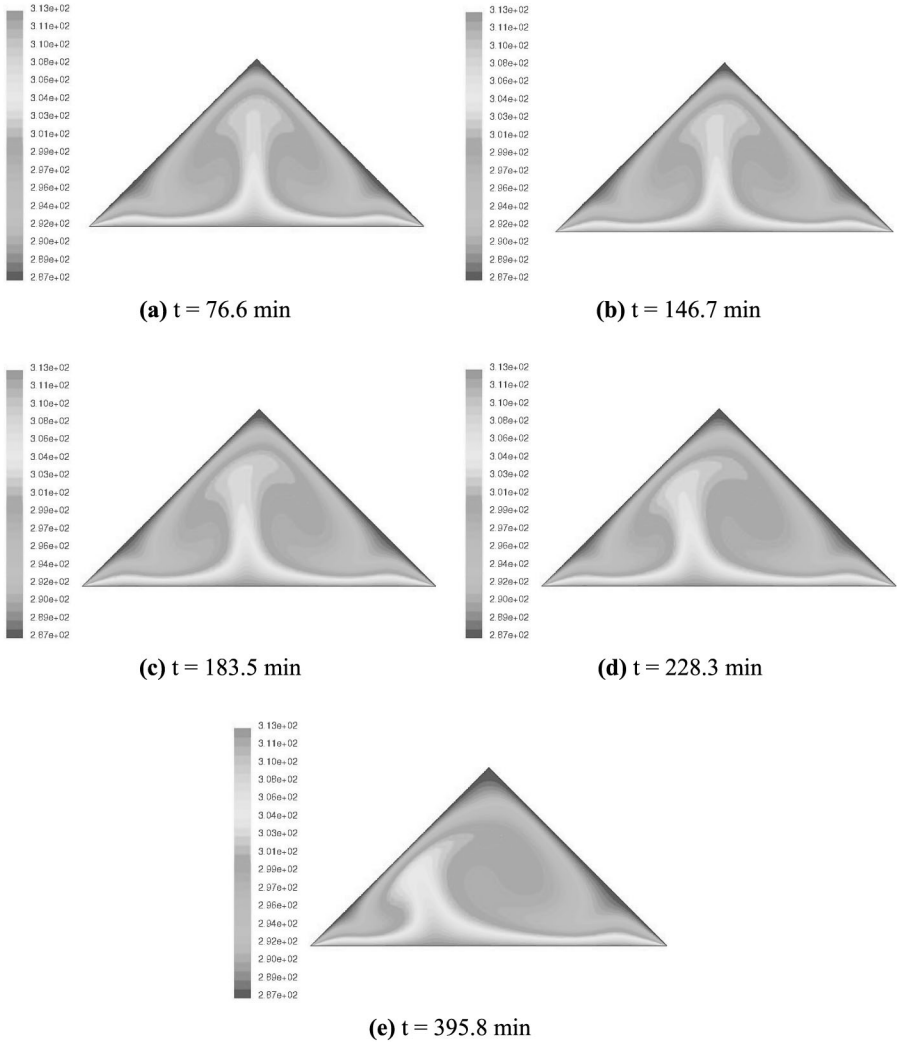


**Figure 13.**
Temporal evolution of the flow structure during the transition from a symmetrical steady-state condition to an asymmetrical steady-state condition at $Gr_{H,C}$

The temperature at the central region of the cavity was susceptible to geometry changes and also to modifications in the two aspect ratios. In term of heat transfer, at a small aspect ratio ($A = 1$), the RT cavity is capable of transferring 8.7 percent more heat compared to the IT and 71 percent more compared to the RE under the conduction regime ($Gr_H = 10^3$). The heat transfer enhancement is not as notorious for the natural convection regime, they drop to 3 and 29 percent ($Gr_H = 10^6$) compared to IT and RE, respectively. Conversely at $A = 2$, the IT is found to be the best for purposes of heat transfer through the horizontal base wall. Compared to the related RT and RE cavities, the benefits inherent to the IT is 28 and 107 percent in the conduction regime, dropping down to 13 and 31 percent at high $Gr_H = 8 \times 10^5$.

## References

Campo, A. and Ridouane, E.H. (2005), "Enhancement of natural convection transport in slender right-angled triangular cavities by way of molding the upper wall", *J. Enhanced Heat Transfer*, Vol. 12, pp. 327-41.

Corcione, M. (2003), "Effects of the thermal boundary conditions at the side walls upon natural convection in rectangular enclosures heated from below and cooled from above", *Intern. J. Thermal Sciences*, Vol. 42, pp. 199-208.

De Vahl Davis, G. (1983), "Natural convection of air in a square cavity: a benchmark numerical solution", *Intern. J. Numer. Meth. Fluids*, Vol. 11, pp. 249-64.

Flack, R.D. (1980), "The experimental measurement of natural convection heat transfer in triangular enclosures heated or cooled from below", *ASME J. Heat Transfer*, Vol. 102, pp. 770-2.

*FLUENT Reference Manual* (2002), FLUENT Inc., 10 Cavendish Court, Centerra Resource Park, Lebanon, NH.

Gebhart, B., Jaluria, Y., Mahajan, R.L. and Sammakia, B. (1988), *Buoyancy-Induced Flows and Transport*, Hemisphere, New York, NY.

Holtzmann, G.A., Hill, R.W. and Ball, K.S. (2000), "Laminar natural convection in isosceles triangular enclosures heated from below and symmetrically cooled from above", *ASME J. Heat Transfer*, Vol. 122, pp. 485-91.

Jaluria, Y. (2003), "Natural convection", in Bejan, A. and Kraus, A.D. (Eds), *Heat Transfer Handbook*, Chapter 7, Wiley, New York, NY.

Raithby, G.D. and Hollands, K.G.T. (1998), "Natural convection", in Rohsenow, W.M. *et al.* (Eds), *Handbook of Heat Transfer*, 3rd ed., Chapter 4, McGraw-Hill, New York, NY.

Salmun, H. (1995), "Convection patterns in a triangular domain", *Intern. J. Heat Mass Transfer*, Vol. 38, pp. 351-62.

Tannehill, J.C., Anderson, D.A. and Pletcher, R.H. (1997), *Computational Fluid Mechanics and Heat Transfer*, Taylor and Francis, Washington, DC.

## Corresponding author

El Hassan Ridouane can be contacted at: eridouan@cems.uvm.edu